ACS APPLIED MATERIALS & INTERFACES

www.acsami.org

Research Article

Mechanical Stimulation of Adhesion Receptors Using Light-Responsive Nanoparticle Actuators Enhances Myogenesis

Allison N. Ramey-Ward, Hanquan Su, and Khalid Salaita*

Cite This: https://dx.doi.org/10.1021/acsami.0c08871

Read Online

ACCESS | Metrics & More | Article Recommendations | Supporting Information

ABSTRACT: The application of cyclic strain is known to enhance myoblast differentiation and muscle growth in vitro and in vivo. However, current techniques apply strain to full tissues or cell monolayers, making it difficult to evaluate whether mechanical stimulation at the subcellular or single-cell scales would drive myoblast differentiation. Here, we report the use of optomechanical actuator (OMA) particles, comprised of a ∼0.6 μm responsive hydrogel coating a gold nanorod (100 × 20 nm) core, to mechanically stimulate the integrin receptors in myoblasts. When illuminated with near-infrared (NIR) light, OMA nanoparticles rapidly collapse, exerting mechanical forces to cell receptors bound to immobilized particles. Using a pulsed illumination pattern, we applied cyclic integrin forces to C2C12 myoblasts cultured on a monolayer of OMA particles and then measured the cellular response. We found that 20 min of OMA actuation resulted in cellular elongation in the direction of the stimulus and enhancement of nuclear YAP1 accumulation, an effector of ERK phosphorylation. Cellular response was dependent on direct conjugation of RGD peptides to the OMA particles. Repeated OMA mechanical stimulation for 5 days led to enhanced myogenesis as quantified using cell alignment, fusion, and sarcomeric myosin expression in myotubes. OMA-mediated myogenesis was sensitive to the geometry of stimulation but not to MEK1/2 inhibition. Finally, we found that OMA stimulation in regions proximal to the nucleus resulted in localization of the transcription activator YAP-1 to the nucleus, further suggesting the role of YAP1 in mechanotransduction in C2C12 cells. These findings demonstrate OMAs as a novel tool for studying the role of spatially localized forces in influencing myogenesis.

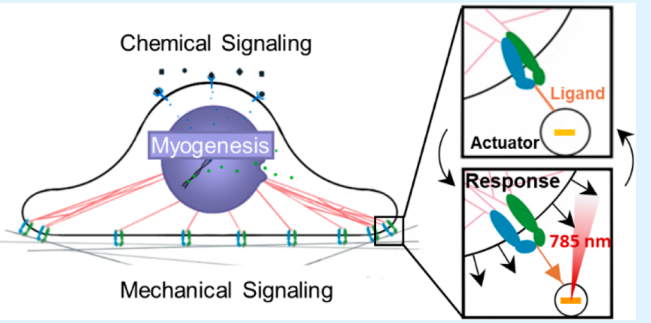

KEYWORDS: *responsive materials, myogenesis, mechanobiology, cyclic strain, differentiation*

INTRODUCTION

Myogenesis is the process of muscle tissue formation, starting from committed myogenic progenitor cells that grow, differentiate, and eventually fuse into myotubes, which become contractile myofibers.[1] This process is sensitive to several external signaling cues which have been extensively studied, and these include a variety of growth factors and cytokines.[2] For example, insulin-like growth factor triggers MEK pathway activation in early myogenic differentiation, and the MEK/ERK pathway has long been known to be crucial in myogenic commitment.[3,4] Interestingly, the mechanical and physical environment also complements chemical inducers to mediate myogenesis, and the role of such physical cues is less studied because of a lack of methods to investigate this aspect of muscle biology.

The composition and stiffness of the muscle environment are shown to impact myogenesis in vitro and in vivo with substrates closely mimicking the native tissue facilitating muscle formation.[5,6] This result has been further validated by the reduction of functional maturation in cells with aberrant extracellular attachment, particularly those lacking certain integrin receptors.[7] McClure and colleagues demonstrated that aligned substrates enhance differentiation and fusion, even in these mutated cells, highlighting the importance of cell–substrate interactions in skeletal muscle biology.[8] Further efforts to study the role of physical cues in myogenesis use hydrogels to apply stresses to cultured cells. This can be accomplished using micropillars to apply stress to gel culture substrates[9] or by culturing precursor cells on statically strained substrates.[10] These efforts highlight the role of novel materials in advancing our understanding of the interplay between mechanics and muscle cell biology. Yet another aspect of mechanical signaling relevant to the native physiology is the role of dynamic mechanical loading. Transient contraction of myofibers places the muscle tissue under mechanical stress for

Received: May 14, 2020
Accepted: July 9, 2020
Published: July 9, 2020

brief and repeated durations in situ, which may have a signaling role that is distinct from that of static mechanical strain.

Indeed, physical therapy and exercise have been observed for decades to improve muscle mass and function in patients with musculoskeletal conditions,[11−13] raising the question of if and how dynamic mechanical stimuli promote myogenesis. To address this, cyclic strain bioreactors (CSBs) have been employed to apply controlled stretch to monolayers of muscle cells cultured on polymeric substrates modified with cell adhesion ligands. Studies have shown increased expression of myogenic differentiation factors on CSBs as compared to static, unstrained substrates.[14] In addition, application of uniaxial cyclic strain to myoblasts significantly enhanced their alignment[15] and can rescue the differentiating phenotype in cells treated with a myotube formation inhibitor.[16] Similar results have been demonstrated in other cell types, where actuatable pillar arrays can direct the elongation and alignment of mesenchymal cells, indicating the importance of tools to study these ubiquitous cellular responses to strain.[17]

An important and fundamental question that remains in this area is whether subcellular mechanical stimulation of myogenic progenitor cells can trigger the same enhanced differentiation that is demonstrated by bulk cyclic strain experiments. One possibility is that these cells are insensitive to subcellular mechanical stimulation and that whole-cell inputs are required to mediate activation of these pathways. Alternatively, activation of low copy numbers of intercellular signaling molecules may be sufficient to mediate the response. A related question pertains to the orientation and spatial distribution of the mechanical trigger and if myoblasts recognize the orientation of a subcellular stimulus to produce a "polarized" response similar to the alignment seen with CSBs. These questions are currently challenging to address with existing technologies because CSBs have limited spatial control of mechanical stimulation, applying only uniaxial or biaxial strain with little ability to study unique geometries. In contrast, atomic force microscopy (AFM) and magnetic tweezer techniques control mechanics with single-molecule resolution[18,19] but cannot access the basal side of the cell where adhesions are formed.

To address these questions of cellular responses to spatially controlled force application, we employed optomechanical actuators (OMAs). These are near-infrared (NIR)-responsive composite nanoparticles with a gold nanorod (AuNR) core (λ_{abs} 785 nm) surrounded by a thermoresponsive polymer shell that was covalently modified with cell adhesion ligands. When illuminated with NIR light, the core of the particle heats up, and this highly localized temperature change radially extends to the polymer shell. This causes the polymer shell to collapse, pushing water out of the hydrogel at the nanosecond to microsecond time scales. Upon removal of the NIR stimulus, the particle rapidly reswells to its original size.[20] OMAs have previously been demonstrated to optically control receptor tension at the cell surface with high spatiotemporal accuracy.[21] In this work, we applied the unique properties of OMAs to study if subcellular mechanical stimulation would enhance differentiation of myoblasts in vitro. We demonstrate enhancement of short- and long-term indicators of myogenesis resulting from OMA stimulation: cell elongation, unidirectional alignment, fusion, and myosin expression. Interestingly, both the stimulation frequency and the geometry of force application caused differential responses in C2C12 myoblasts. We also sought to understand the mechanism of this mechanically driven myogenesis, finding a role for increased YAP1 nuclear localization, which is known to be mechanotransductive and acts in the MEK/ERK myogenic signaling pathway. This work demonstrates OMAs as a novel, light-driven tool for studying the role of subcellular cell−substrate mechanics in biomaterial applications.

EXPERIMENTAL SECTION

Optomechanical Actuator Synthesis. OMAs were synthesized as described previously.[21] Gold seed solution was synthesized from 0.5 mM $HAuCl_4$ (Acros Organics, Thermo Fisher Scientific, Waltham, MA) in 0.2 M hexadecyltrimethylammonium bromide (CTAB) (TCI, Japan) followed by adding 6 mM cold $NaBH_4$ (Sigma-Aldrich, St. Louis, MO) and vigorously stirred for 2 min. For gold nanorod synthesis, 4 mM $AgNO_3$ (Sigma-Aldrich) was added to a growth solution of 3.6 g of CTAB and 0.4936 g of sodium oleate (NaOL) (TCI) in 100 mL of water. After 15 min, an equal volume of 1 mM $HAuCl_4$ was added and vigorously stirred for 90 min, after which the solution was acidified with 0.6 mL of 12.1 M HCl (EMD Millipore, Burlington, MA). After 15 min of gentle stirring, 0.6 mL of 0.064 M ascorbic acid (Fisher Scientific) was stirred in; then 80 μL of the seed solution was added. The final solution was stirred for 30 s and then allowed to sit at 30 °C for 12 h to grow AuNRs with NIR absorption at 785 nm (as characterized by UV−vis−NIR spectra). AuNRs were purified by centrifugation at 5000 rpm and washed with Milli-Q water.

To prepare AuNRs for polymer encapsulation, CTAB was partially displaced with a vinyl-terminated adsorbate by combining 20 mg of *N,N′*-bis(acryloyl)cystamine dissolved in 10 mL of ethanol, and prepared AuNRs were concentrated to 90 mL. The mixture was vigorously stirred at 700 rpm for at least 12 h, purified by centrifugation at 5000 rpm, and resuspended in 15 mL of Milli-Q water.

OMA synthesis was performed by first heating 15 mL of Milli-Q water to 70 °C with N_2 gas purging in a three-neck flask. Subsequently, 0.1 g of *N*-isopropylmethacrylamide (NIPMAm) (Aldrich) and 0.01 g of *N,N′*-methylenebis(acrylamide) (Sigma-Aldrich) were added, followed by 1 mL of vinyl-modified AuNR solution under continuous stirring and N_2 flow. NIPMAm polymerization was initiated after 1 min with 80 μL of 0.1 M 2,2′-azobis(2-methylpropionamidine) dihydrochloride (AAPH) (Aldrich) and allowed to polymerize for 2 h. Alkyne functional groups were introduced by adding 30 μL of propargyl methacrylate (Alfa Aesar, Haverhill, MA) in 1 mL of ethanol after 2 h and allowing the reaction to proceed for an additional hour. The solution was then cooled to room temperature, purified at least 2 times by centrifugation at 5000 rpm for 1 h, and redispersed in Milli-Q water to remove gold-free polymer nanoparticles. Final OMAs were resuspended in 4 mL of Milli-Q water.

OMA Characterization. OMA size, thermoresponsivity, and AuNR incorporation were verified with transmission electron microscopy (TEM) (HT-7700 120 kV TEM, Hitachi, Japan), dynamic light scattering (DLS) (NanoPlus Zeta/Particle Analyzer, Particulate Systems, Norcross, GA), and spectrophotometry (Lambda 35 UV−vis Spectrophotometer, PerkinElmer, Waltham, MA), respectively. NIR responsivity was visualized by adding azide-modified FAM dye (Lumiprobe, Cockeysville, MD) to the alkyne-coated particles by copper-catalyzed click reaction and imaged with fluorescence microscopy.

Optical Imaging. All optical imaging in this work was conducted using a Nikon Eclipse Ti microscope (Nikon, Japan) running the NIS Elements software (version 4.13.05, Nikon) with an Evolve electron-multiplying charge-coupled device (EMCCD) (Teledyne Photometrics, Tucson, AZ) and epifluorescence source (Intensilight, Nikon). Filter cubes were used for fluorescent imaging: TRITC, FITC, AT-DAPI, and RICM (Nikon). A NIR filter cube (Chroma) was also used to reduce background due to the NIR source. Imaging was performed with 20×, 40×, or 100× objectives (Nikon).

https://dx.doi.org/10.1021/acsami.0c08871
ACS Appl. Mater. Interfaces XXXX, XXX, XXX−XXX

Surface Preparation. All experiments were performed on glass slides covalently modified with OMAs and cell adhesion ligands (Figure S1a). Briefly, 25 mm glass cover slides (#2, VWR, Radnor, PA) were cleaned by sonication in ethanol and Milli-Q water for 10 min each. Subsequently, slides were immersed in piranha solution (3:1 H_2SO_4(EMD Millipore):H_2O_2(Sigma-Aldrich)) for 20 min to expose silane groups on the glass. ***Caution**: piranha solution can be explosive when mixed with organics.* Slides were washed thoroughly in Milli-Q water and then incubated at room temperature overnight in 1% 6-azidosulfonylhexyltriethoxysilane (Gelest, Morrisville, PA) in acetone to introduce azide groups. Surfaces were rinsed in Milli-Q water and dried under N_2 gas; then OMAs were covalently bound to the surface using copper-catalyzed click chemistry. A 7.5 μL amount of 2:1 THPTA (Lumiprobe):$CuSO_4$ (Mallinckrodt, Phillipsburg, NJ) solution, 7.5 μL of 10 mM sodium ascorbate (Sigma-Aldrich), and 50 μL of prepared OMAs were sandwiched between two azide-functionalized surfaces for 2 h at room temperature or overnight at 4 °C.

To prepare for cell culture, surfaces were functionalized with cyclic RGDfk (Arg-Gly-Asp-Phe-Lys−PEG-PEG). A 500 μg amount of cRGDfk (Peptides International, Louisville, KY) was modified with an azide functional group by combining with excess of NHS-azide (Thermo Scientific) in 20 μL of DMSO (EMD Millipore) at room temperature for 12 h. Product was purified by reverse-phase HPLC (Figure S1b). OMA surfaces were washed in Milli-Q water and modified with cRGDfk-N_3 through copper-catalyzed click chemistry (7.5 μL of 2:1 THPTA:$CuSO_4$, 7.5 μL of sodium azide, 2 μL of 300 mM cRGDfk-N_3, 40 μL of 55% v/v DMSO per 2-surface sandwich) overnight at 4 °C. Surfaces were stored in 2-surface sandwiches at 4 °C until use.

In some cases, an azide-modified fluorescein (FAM) was added to surfaces and cells were seeded to verify cell−surface binding and evaluate the surface integrity over time (Figure S1d,e).

Cell Culture and Transfection. C2C12 myoblasts were cultured in myoblast growth media (Dulbecco's Modified Eagle Medium (DMEM) (Corning, Corning, NY), 10% fetal bovine serum (FBS) (Corning), and 1% penicillin/streptomycin (P/S) (Corning)), which was changed every 48 h, and maintained at 37 °C and 5% CO_2. For experiments, cells were passaged no more than 15 times before plating. Prepared surfaces were fitted into metal imaging chambers and submerged in 1% P/S for 30 min at 37 °C before plating cells to remove bacteria and equilibrate temperature. Cells were seeded onto surfaces at a density of 30 000 cells/surface and allowed to attach overnight before experiments. For 5-day myogenesis experiments, medium was changed to myogenic media (DMEM, 2% horse serum (Corning), 1% P/S) when cells reached 80% confluency and was changed daily.

Transfection was performed following protocols developed elsewhere for C2C12 myoblasts.[22] Briefly, for each surface, 500 ng of m-cherry LifeAct plasmid or 1 μg of pEGFP-C3-hYAP1 (gifted to Addgene by Marius Sudol, Addgene Plasmid #17843[23]) was added to 100 μL of Opti-MEM (Gibco, Waltham, MA) and 2 μL of Lipofectamine 2000 per μg of DNA (Invitrogen, Waltham, MA), mixed by pipetting, and incubated at room temperature for 25 min. The DNA solution was then added to each surface concurrent with cell plating and incubated overnight before imaging. During subsequent NIR stimulation, cells were kept at room temperature for the duration of the stimulation and then returned to 37 °C.

Mechanical Stimulation in Myoblast Elongation. Stimulation of OMAs was performed in all experiments using a UGA-42 Firefly galvo mirror illumination system (Rapp OptoElectronic, Germany) with the ROE Syscon-NIS software (version 1.1.9.9, Rapp Opto-electric) to spatiotemporally control a 785 nm NIR laser at 15 mW power. M-cherry LifeAct-transfected cells were stimulated with a 5 μm NIR laser spot placed near the edge of the cell for 20 min under the following conditions: 100 Hz (90% duty cycle), 10 Hz (50% duty cycle), continuous (NIR on, no oscillation), or unstimulated (no NIR illumination). A different duty cycle was selected for 100 Hz to provide enough laser on time to ensure particle collapse. Cells were imaged at 100× magnification every 5 min. Extension of cells in the direction of NIR stimulation was quantified using ImageJ.

Mechanical Stimulation in Myogenesis. Cells were seeded onto modified surfaces with an "X" scratched onto the back of the slide with a diamond scribe to serve as a visual marker to ensure repeated NIR stimulation of the same region (Figure S2a,c). This was achieved by mechanically actuating myoblasts with an array of 9 evenly spaced, uniformly timed 100 ms NIR illumination sites that were triggered at a frequency of 1.1 Hz at each location for 20 min every other day over a duration of 5 days (Figure S2b,c) with patterned stimulation consisting of laser spots arranged in the following geometries: 1 line (linear array consisting of 9 uniformly spaced spots), 2 lines (2 linear arrays of 9 uniformly spaced spots), or a circle (an approximately 60 μm diameter circular array of 9 uniformly spaced spots). To determine the role of MEK/ERK signaling (a known pathway in early myogenesis in vitro and in vivo) in mechanically stimulated myogenesis, some surfaces were treated with 10 μM of MEK1/2 inhibitor U0126 (Cell Signaling Technology, Danvers, MA) or vehicle (dimethyl sulfoxide (DMSO)) in media changed every other day, 1 h before mechanical stimulation (Figure S2b).

In one specific case, cells were stimulated every day instead of every other day to evaluate the sensitivity of the cellular response, as discussed below.

Immunocytochemistry. After 5 days, cells were washed in phosphate-buffered saline (PBS 1×) and fixed in 4% formaldehyde (Sigma-Aldrich) in PBS at room temperature for 20 min. Cells were then permeabilized for 10 min in 0.1% Triton X-100 (Sigma) in PBS and then washed 3 times in PBS. To reduce nonspecific antibody binding, surfaces were blocked for 30 min in 1% w/v bovine serum albumin (BSA) (Roche, Switzerland) with 22.5 mg/mL glycine in PBS with 0.1% Tween 20 (Sigma) (PBS-T) followed by triplicate washes in PBS. For sarcomeric myosin staining, anti-MF20 (contributed to Developmental Studies Hybridoma Bank by Fischman, D.A., DSHB product MF20[24]) was diluted 1:2 in dilution buffer (1% BSA in PBS-T) and incubated overnight at 4 °C. Excess antibody was removed with triplicate washes of PBS, and goat antimouse Alexa555 secondary antibody (Molecular Probes, Eugene, OR) was applied at 1:1000 in dilution buffer for 1 h at room temperature. Cells were counterstained with Phalloidin-iFluor 488 (Abcam, UK) for 20 min at room temperature to visualize actin. Cells were then imaged at 20× and 40× magnification. For analysis of phosphorylated ERK expression, surfaces were stimulated and harvested as described in Figure S2b and stained using the protocol described above with a phosphor-p44/42 MAPK (Erk1/2) (Thr202/Tyr204) primary antibody (Cell Signaling Technology, Danvers, MA) diluted 1:250 and goat antirabbit Alexa 555 secondary antibody (Molecular Probes, Eugene, OR) at 1:1000 dilution. All cells were counterstained with NucBlue (Molecular Probes) to visualize nuclei, prepared as recommended in dilution buffer, to visualize nuclei.

Alignment and Differentiation Analysis. The degree of cellular differentiation was determined by evaluating the relative alignment of myocytes and myotubes and quantifying MF20 myosin staining. Cell angles were measured using ImageJ (NIH, Rockville, MD) in stimulated and unstimulated regions of each surface, referencing bright-field, actin, and myosin staining images to identify individual cell boundaries. Cells that lacked clearly identifiable boundaries were excluded from the analysis to ensure the accuracy of the angle measurements. The average alignment angle with a 95% confidence interval and dispersion vector were calculated for each region. Myosin staining was quantified as the ratio of nuclei contained in MF20 positive staining cells to total nuclei in stimulated and unstimulated regions of each surface. The fusion index was calculated as the average number of nuclei per cell in stimulated and unstimulated regions. In some cases, cells appeared to be overlapping, and a single nucleus could not be attributed to one cell. These cells were excluded from fusion index measurements but were included in myosin quantification only if both overlapping cells were myosin positive. Finally, to ensure any observed differences were not a function of cell density or

https://dx.doi.org/10.1021/acsami.0c08871
ACS Appl. Mater. Interfaces XXXX, XXX, XXX−XXX

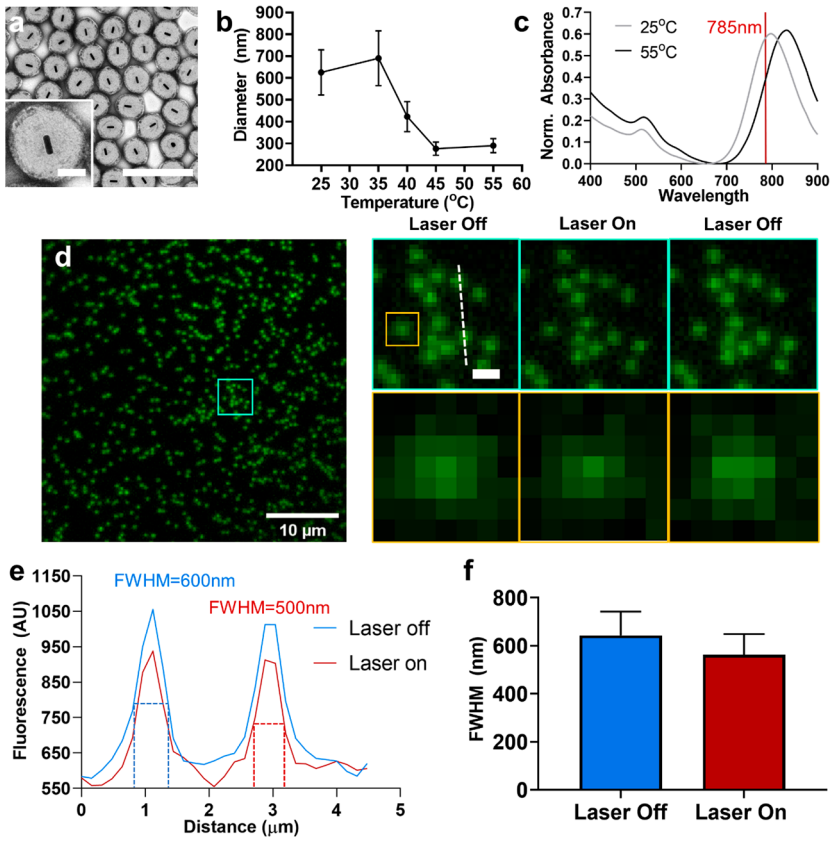

Figure 1. Optomechanical actuator (OMA) characterization. (a) Representative TEM shows OMAs with uniform incorporation of an AuNR core. Scale bar = 1 μm, inset scale bar = 200 nm. (b) Temperature-dependent dynamic light scattering (DLS) shows the hydrodynamic diameter and temperature responsiveness of OMAs with an estimated LCST of 40 °C. Each data point shows the mean hydrodynamic diameter from 20 measurements on each of the two independent OMA preparations. Bars show the range of the data. (c) UV−vis−NIR spectrophotometry at two temperatures (25 and 55 °C). Heating above the LCST shows a red shift of the absorbance. Red line indicates the wavelength of NIR illumination in our work. (d) (Left) For purposes of particle characterization, a sparse density of FAM-labeled OMAs were attached to a glass surface. Scale bar = 10 μm. (Right, top) Fluorescence images of OMAs labeled with FAM before and after NIR illumination. Scale bar = 1 μm. (Right, Bottom) A single particle zoom-in is shown. (e) Line scan of two OMA particles (white dashed line in image) shows a decrease in particle fluorescence in the laser spot area as well as a ∼100 nm change in particle diameter as measured by the full width at half-maximum (fwhm) of the particle fluorescent signal. (f) This is further quantified over n = 25 OMAs with an average change in diameter calculated at 93 nm. Bar graph shows mean ± standard error of the mean over 3 independently prepared surfaces.

proliferation, the number of cell nuclei in each region of interest was quantified.

Alignment, MF20 expression, and fusion were also compared in treatment and control groups in MEK1/2 inhibition experiments.

To eliminate cell density as a confounding factor in myogenesis quantification, cells were fixed and stained with NucBlue at Day 1, Day 3, and Day 5, and the average number of nuclei was quantified in stimulated and unstimulated regions.

Mechanism of Mechanotransduction in Optomechanical Actuation. To investigate YAP translocation, C2C12 cells were plated onto OMA surfaces, transfected with an eGFP-YAP1 plasmid, and counterstained with Hoescht 33342 dye prior to experimentation. Single cells were stimulated at multiple points in the nucleus or cytoplasm at 10 Hz or exposed to continuous NIR light for 20 min. Cells were imaged at 100× magnification to visualize the change in relative fluorescent intensity between the nuclear and the cytoplasmic YAP signal and compared to unstimulated cells. In phosphorylated ERK staining experiments, a positive signal was quantified as the average fluorescent intensity in each field of view.

Statistical Analysis. Summary data are presented as box plots showing the range of data and individual points unless otherwise stated. Cells were measured and data compiled across three independently prepared surfaces for all experiments unless otherwise noted. For actin extension quantification, all cells were combined and summary statistics are shown. For alignment analysis, angle measurements of individual cells from multiple stimulated and unstimulated regions are compiled to determine the significance of alignment. Myosin and fusion data points are presented as the quantification of each stimulated/unstimulated region of interest. YAP quantification shows the behavior of individual cells in each treatment condition. Each data set was evaluated for parametric assumptions (normality, equal variances), and appropriate parametric or non-parametric tests were performed. Statistical testing was conducted in Prism7 (GraphPad, San Diego, CA) with the exception of alignment data, which was analyzed in MATLAB (MathWorks, Natick, MA) using the Circular Statistics Toolbox.[25]

RESULTS AND DISCUSSION

Surface Characterization. We first sought to characterize the structure and response of OMA particles. TEM showed that OMAs were 360 ± 40 nm in diameter with uniform incorporation of 100 ± 6 nm × 20 ± 7 nm AuNRs within their core (Figure 1a), as previously described.[21] Because TEM is performed dry under vacuum, it underestimated the size of OMAs under the experimental conditions. Therefore, we further used temperature-dependent dynamic light scattering (DLS) to measure the hydrodynamic size of OMAs and found that, though particles used in this study were prepared

https://dx.doi.org/10.1021/acsami.0c08871
ACS Appl. Mater. Interfaces XXXX, XXX, XXX−XXX

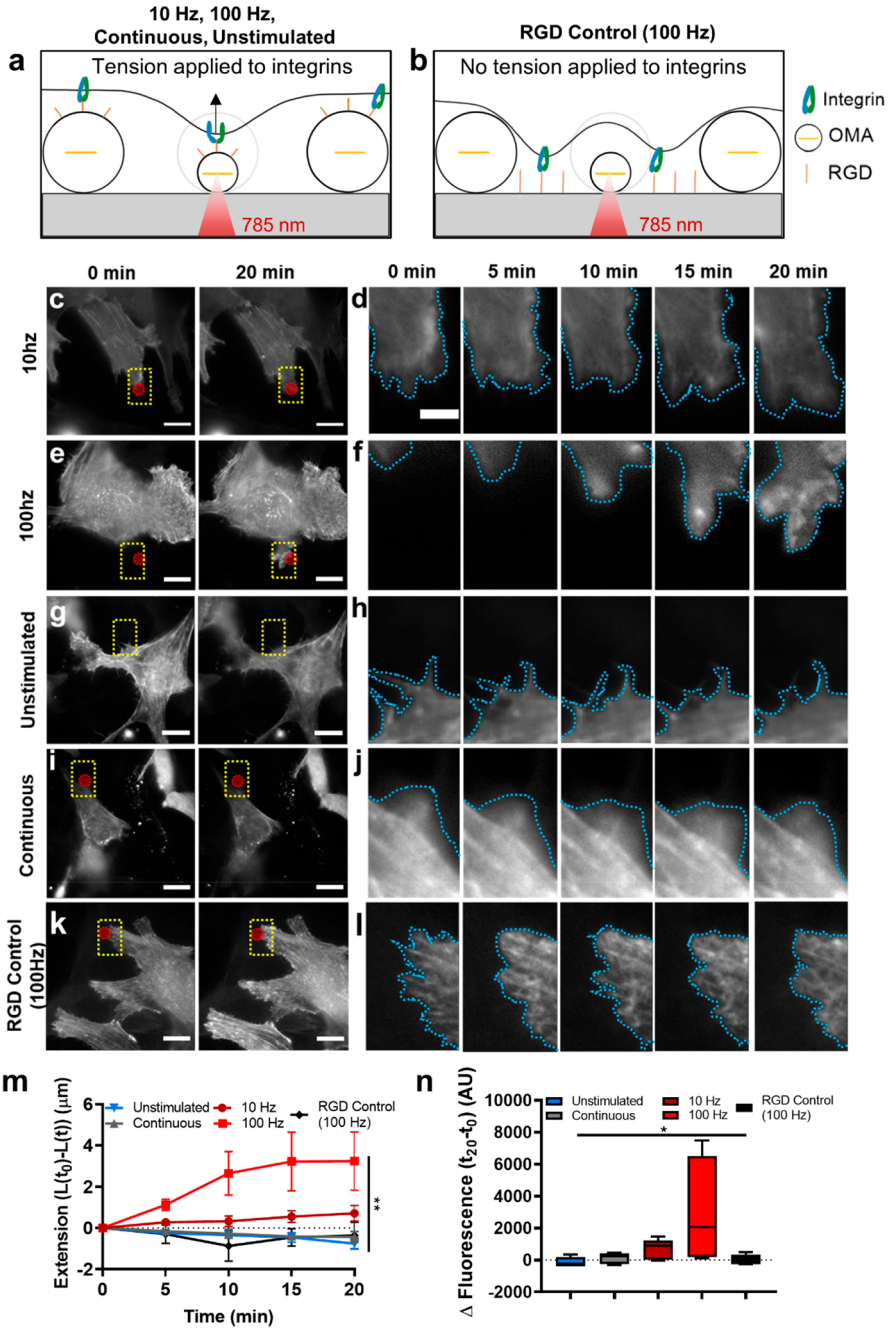

Figure 2. Mechanical actuation directs cellular extension. (a) Schematic of the surfaces used for the 10 Hz, 100 Hz, unstimulated, and continuous stimulation conditions in these experiments, showing direct force application to cellular integrins through OMA-bound RGD. (b) Schematic of surfaces used in the RGD control group experiments, showing cell attachment to the glass surface and no force transmission from OMA actuation. Schematics are not to scale. (c–l) Representative fluorescence images of C2C12 myoblasts transfected with m-Cherry LifeAct and stimulated with NIR at 10 Hz (c and d), 100 Hz (e and f), nonstimulated (g and h), and continuously stimulated (i and j) and the RGD control stimulated at 100 Hz (k and l). NIR stimulation was performed with 15 mW power in the region indicated with a red circle. Scale bars = 15 μm, outset scale bar = 5 μm. Yellow box regions indicate zoom in shown to the right. Blue dotted lines indicate the edge of the cell. (m) Plot of mean cell extension as a function of NIR stimulation time. Error bars represent the standard deviation from n = 7 independently prepared surfaces (n = 3 surfaces for RGD control) with n = 7 cells. Groups were compared using a mixed-effects model on n = 7 for each condition. (**) $p < 0.01$. (n) Cells were also quantified for mean actin polymerization in the stimulated region of interest. Error bars represent the standard deviation from n = 7 independently prepared surfaces (n = 3 for RGD control). (*) $p < 0.05$ by the Kruskal–Wallis test.

following the protocol previously published by this lab,[21,26] the OMAs in this paper were found to have a slightly (~20%) larger hydrodynamic diameter, 630 ± 103 nm at room temperature, than previously reported, possibly due to differences in the preparation, reagents, or DLS instrument used. Notably, the collapsed diameter was comparable to our original report, measured by DLS to be an ~50% reduction in hydrodynamic diameter to 290 ± 32 nm upon heating to 55 °C. This decrease was significant and showed a lower critical solution temperature (LCST) of 40 °C, comparable to other

https://dx.doi.org/10.1021/acsami.0c08871
ACS Appl. Mater. Interfaces XXXX, XXX, XXX–XXX

reports[21,27,28] (Figure 1b). Incorporation of AuNRs within the OMA core was further verified with UV−vis−NIR absorbance, which showed two peaks at 789 and 512 nm (Figure 1c), corresponding to the expected AuNR longitudinal and transverse surface plasmon resonance. A red shift in the absorption spectra was observed above the LCST, thus verifying the change in the local environment around the AuNR following the LCST transition.

To measure OMA optical response to NIR light, particles were covalently bound to a glass substrate and then stimulated at 785 nm. The fluorescein (FAM) emission was reduced under NIR light (∼45%), as previously reported, with a corresponding decrease in particle full-width half-maximum (fwhm) from 643 ± 98 to 562 ± 86 nm (Figure 1d−f), though it is important to note these measurements are diffraction limited. The observed actuation response was highly reversible and repeatable over at least 1200 illumination cycles (20 min) (Videos S1 and S2).

On the basis of the diffraction-limited surface collapse measurements, the change in particle diameter on the surface leads to an estimated strain (in the plane of the surface) on the order of 15%. Previous data using AFM shows anisotropic collapse of OMAs with increasing temperature with an approximately 30% decrease in height and 17% decrease in width.[21] Depending on the location of the bound RGD molecule on the OMA surface, cell receptors in our system experience 15−30% substrate strain. This is a significantly lower magnitude of collapse than observed by DLS in solution, as covalent tethering of the OMA to the glass flattens the particle and constrains its motion, limiting the change in diameter. A wide range of substrate strain has been employed in the CSB literature, promoting myogenesis in myoblasts and stem cells from 3% to 15% strain[14,15,29−31] yet inhibiting it at bulk substrate strains of 20%.[32] However, these studies are performed with bulk strain systems, meaning every bound integrin in the cell experiences these strains rather than just a subset of them. Our data indicate myoblasts have a pro-myogenic response to higher substrate strains applied on smaller spatial scales, a novel finding resulting from our technology.

Finally, we wanted to verify the compatibility of these surfaces for studying myoblasts. Reflection interference contrast microscopy (RICM) shows that the glass surfaces were uniformly coated in OMAs following the procedure described above (Figure S1c), and addition of C2C12 myoblasts to these surfaces did not disrupt the OMA layer (Figure S1d,e).

Myoblasts Produce Local Protrusions in Response to Optomechanical Stimulation. To test if OMAs are appropriate for driving myogenesis, we examined F-actin-based cellular elongation, one of the first morphologic signals of myogenesis.[33] Single-point NIR (5 μm) stimulation on OMAs was performed at varying frequencies on m-cherry LifeAct-transfected C2C12s. Cells were first cultured on surfaces coated in RGD-modified OMAs (Figure 2a). Cells responded to short-term (20 min) cyclic stimulation by generating actin-rich protrusions in the direction of the stimulus at both 10 and 100 Hz (Figure 2c−f) in the direction of the force. This is in agreement with this lab's previous work in fibroblasts, which demonstrated extension and migration of cells in the direction of the NIR stimulus at 10 Hz,[21] and accordingly a greater response was seen at frequencies an order of magnitude higher (100 Hz). However, the 100 Hz frequency is not biologically relevant, and indeed, other studies of cyclic strain typically apply stretch in the 0.1−1 Hz range.[14,16,29,34] The results seen in this study may be a reflection of the brief 20 min stimulation time window as compared to hours of slower stimulation used in other studies.

Cells receiving no NIR light did not respond with significant extension during the 20 min imaging time window (Figure 2g and 2h). Likewise, cells exposed to continuous, noncyclic NIR light showed no significant extension toward the stimulus (Figure 2i and 2j). Other methods of constant force application to cells have resulted in myoblast elongation along the axis of force production. These include shear flow[35] and strained substrate[36] bioreactors as well as composite materials containing stiff pillars.[9] However, these methods applied strain uniformly to the entire cell body and over longer time periods (hours), while OMAs in these experiments provided a highly localized mechanical stimulus over a short time span (minutes). The ability to resolve differential responses in cell morphology on these short time scales in single cells is one advantage of OMAs over bulk CSBs while also maintaining the ability to perform longer term, multiday studies. The lack of response to constant NIR light also demonstrates that the observed cellular responses are not due to the 785 nm laser itself nor any heat accumulated by the AuNRs through NIR absorbance. This does not exclude the possibility that local heating occurs, particularly in conditions with longer NIR on times, only that such heating does not drive the observed response. Though previous modeling of the OMA particle response showed little to no heating at the surface of the particle under NIR illumination,[20,21] future work could employ thermal imaging to determine localized temperature changes or super-resolution microscopy to identify changes in receptor number or activation at the stimulation site.

We next investigated if this extension resulted from direct force transmission to cellular integrin receptors and not from some other mechanical stimulation other than OMA force. For example, collapse of the pNIPMAm OMA shell is driven by the rapid exclusion of water in the hydrogel,[20] which could locally deform the cell membrane and trigger stretch-activated membrane channels to drive a response. To study this, the surface preparation protocol was altered such that the cyclic RGD was attached directly to the glass slide rather than the OMA particle. With this control surface, the OMA is present and active but does not directly bind and transmit force to the cell integrins (Figure 2b). This procedure did not visually affect cell attachment or OMA density on the surface (Figure S3) but did result in statistically less cellular extension in the direction of NIR stimulation at 100 Hz (Figure 2k and 2l). Therefore, OMAs primarily mediate cellular response through direct integrin mechanical stimulation.

Overall, cyclic strain application through integrins at any tested frequency demonstrated cellular extension, and unstimulated and noncyclic (continuous) illumination did not cause a cell response. However, cyclic actuation of OMAs without cellular integrin engagement elicited no cellular response (Figure 2m). The response was statistically significant at all measured time points, as demonstrated by a mixed-effects analysis (time factor p = 0.531, NIR factor p = 0.003, interaction factor p = 0.2822). This response was further supported by increased actin polymerization in groups where cyclic strain was directly applied to cell integrins (Figure 2n),

https://dx.doi.org/10.1021/acsami.0c08871
ACS Appl. Mater. Interfaces XXXX, XXX, XXX−XXX

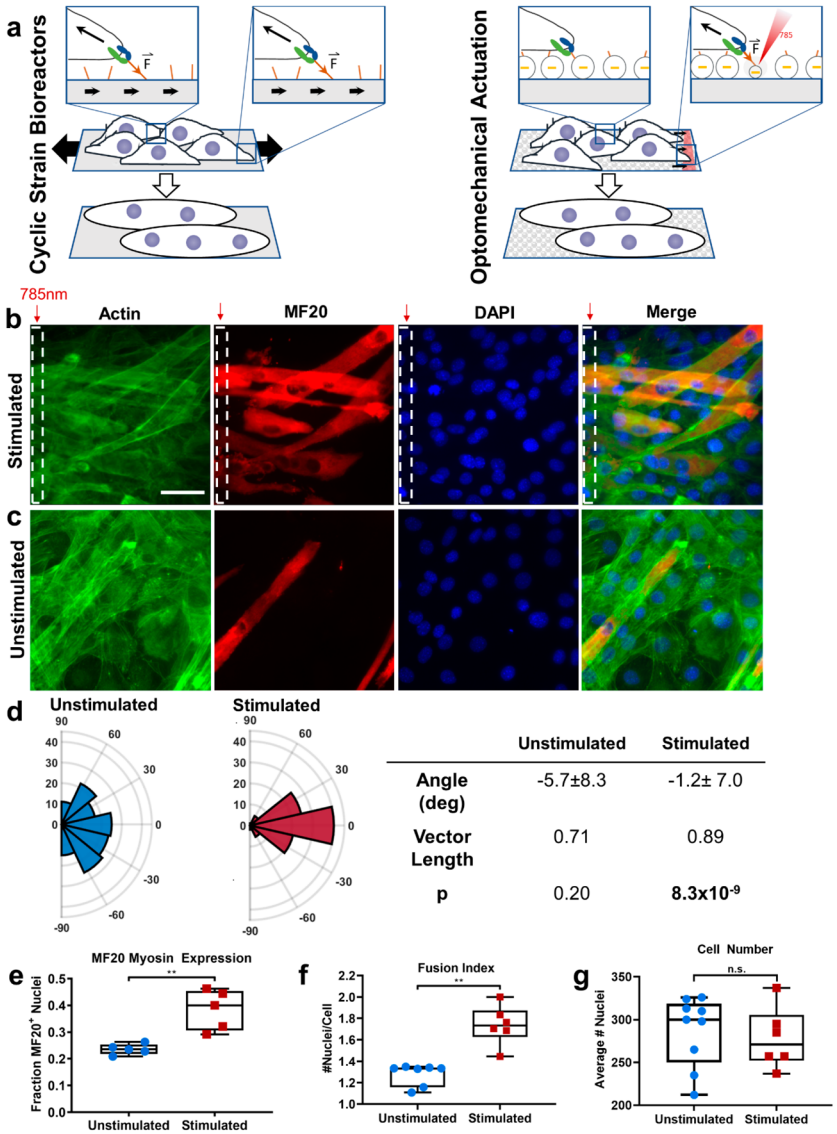

Figure 3. Effect of OMA actuation on myocyte and myotube alignment and sarcomeric myosin expression. (a) Schematic showing cyclic strain bioreactors drive myogenesis with bulk force application (left). This work aims to study the application of cyclic forces at the subcellular length scale using OMAs (right). Schematics are not to scale. (b and c) Representative images of myocytes stained for F-actin (phalloidin, green), sarcomeric myosin (anti-MF20, red), and nuclei (DAPI, blue). Images show regions of myocytes stimulated for 5 days at 1.1 Hz (b) or unstimulated controls (c). Scale bar = 50 μm. White dotted regions and red arrow represent NIR stimulation area. (d) Orientation of cells was measured using bright-field and F-actin staining images and plotted using a polar histogram for stimulated n = 100 cells and unstimulated n = 140 cells that were measured from 3 independent experiments. Summary values of alignment are tabulated, showing an average alignment angle ±95% confidence interval, dispersion vector, and p value, calculated by Rayleigh's modified v-test for uniformity, with a significance level of 0.05. Zero angle was defined as being perpendicular to the long axis of OMA stimulation. (e) Box plot of the fraction of MF20 positive nuclei (quantified from DAPI and MF20 images) in n = 5 microscopic areas (stimulated and unstimulated) from 3 independent experiments. (**) $p < 0.01$ vs unstimulated by a Mann−Whitney nonparametric test. (f) Box plot of the average fusion index (nuclei/cell, quantified by DAPI, F-actin, and MF20 images) in n = 6 stimulated and n = 7 unstimulated areas from 3 independent experiments. (**) $p < 0.01$ vs unstimulated by Mann−Whitney nonparametric test. Bars show range of data in both box plots. (g) Box plot of the average number of nuclei in n = 9 unstimulated and n = 6 stimulated areas from 3 independent experiments, showing that enhanced myogenesis was not a result of different cell numbers by a Mann−Whitney nonparametric test.

significantly different between treatments as demonstrated by a Kruskal−Wallis nonparametric test.

The response of cells to NIR stimulation that is just outside of the cell border (Figure 2e, 2i, and 2k) implies cells also respond to some stimulus from the cell edge. Stimulation locations at or just outside the visible cell edge were originally selected to allow cells to have exposure to the stimulus if they extend several micrometers as previously reported.[21] Cells constantly sample their environment by extending and retracting protrusions from the cell edge. This process may allow the cell to sense OMA collapse outside the cell border, attach, and signal actin polymerization in that direction.

Another possible mechanism for the response of cells to stimuli that are not under the original footprint of the cell is that the contraction of the OMAs results in small amounts of fluid expulsion, which could minorly perturb the nearby (micrometer-scale distance) cell. This could stimulate a slight extension until its integrins engage with RGD ligands on

https://dx.doi.org/10.1021/acsami.0c08871
ACS Appl. Mater. Interfaces XXXX, XXX, XXX−XXX

actuating particles, where a more direct stimulus is applied. Still, the RGD control data (Figure 2k) suggest that it is unlikely to be a parameter in our system and that the main mechanism of this cellular extension is direct integrin engagement."

Indeed, OMAs are reported to have an RGD density of ~2000 molecules/μm^2.[21] The OMA presents only one-half of its surface area for RGD conjugation with the other half bound to the glass slide, resulting in approximately 1200 RGD molecules being available to the cell and 600 integrins binding to each OMA according to some models[37] This calculated density is significantly above the ligand density reported to produce robust integrin adhesion and cell spreading.[38]

While these responses are observable on the time scale of minutes, a point for future investigation could be to study integrin mechanotransduction on the time scale of the OMA force application (nanoseconds) and relaxation (microseconds). This could elucidate whether the cell receptors are constantly adapting to the cyclic application of force in addition to mounting a response over time. Further studies could also measure focal adhesion formation or recruitment of force-sensitive focal adhesion proteins such as talin as another aspect of cell response beyond integrin engagement.

Myosin Expression and Cellular Alignment are Enhanced in Optomechanically Stimulated Cells. In addition to elongation, another important morphological change in myogenesis is the alignment and fusion of differentiating myocytes. Unidirectional alignment of myofibers in vivo optimizes force output during contraction, and inducing alignment using physical substrate properties has been shown to enhance myogenesis.[8,39,40] In addition, Heher and colleagues combined the cyclic strain with passive substrate properties to promote both alignment and differentiation in myoblasts.[36] Therefore, we next evaluated the ability of cyclic strain applied by OMAs to enhance myogenesis in this way (Figure 3a). After 5 days, cells exposed to local NIR stimulation showed significant preferential alignment perpendicular to the axis of linear stimulation compared to unstimulated regions (Figure 3b and 3c). A modified Rayleigh test for uniformity (v test) demonstrated preferential alignment in stimulated cells, while cells not exposed to NIR light did not align in a preferred direction (Figure 3d). NIR-stimulated cells also showed increased expression of MF20 myosin, as evidenced by quantification of positive staining using immunocytochemistry (Figure 3e). As an additional marker of myogenic differentiation, we measured the cellular fusion index (average number of nuclei per cell) and found fusion was significantly enhanced in NIR stimulated myoblasts (Figure 3f). Cell number was also quantified at multiple time points during the experiment, since cell density can be a factor in myoblast differentiation. No differences were found in cell number at any time point between stimulated and unstimulated regions (Figure S2d). The relatively high plating density of myoblasts onto the surfaces likely does not allow for significant proliferation during the stimulation time course.

The high degree of spatial control afforded by the NIR laser allows for the investigation of varying geometries of directional mechanical stimulation applied to myogenic cells. Myoblasts were stimulated with a pattern of two parallel lines for 20 min every other day to see if myogenesis would be enhanced, hypothesizing more cells in the microscopic area would receive the NIR stimulus in this case and accelerate the observed response. However, no differences in myogenesis were observed between the 1-line and the 2-line stimulations, suggesting that cells are very sensitive to this "polarizing" mechanical stimulus and do not require additional stimulation (Figure S4a,c–f). Another potential mechanism in this response is the greater time between repeated stimulation at each point as the laser must move between 18 points instead of 9. This may have dampened any enhanced response the additional stimulation could have caused but would again suggest the sensitivity of C2C12 cells to mechanical stimulation.

While both linear stimulation patterns resulted in perpendicular alignment, cells exposed to circular stimulation showed no evident preferred direction (Figure S4b,d). This pattern was selected to determine if the geometry of the stimulation was important in the observed alignment and differentiation responses or simply the presence of mechanical stimulation. Interestingly, circular patterns of NIR stimulation did not significantly affect MF20 myosin expression (Figure S4e) or fusion (Figure S4f) as compared to unstimulated or linearly stimulated cells. This result was unexpected but not unprecedented. Chandran and colleagues found a change in expression of myogenic markers, including myosin, using equibiaxial strain application instead of uniaxial.[31] This suggests that just the presence of dynamic forces plays a role in promoting myoblast maturation. It is the *orientation* of the stimulus, however, that directs alignment of the resultant myotubes. OMAs provide both mechanical and spatial inputs and allow for unique stimulation geometries and magnitudes to more deeply probe myogenesis.

It was somewhat unexpected that myoblasts would respond significantly to a relatively small region of stimulus relative to the size of the cell. The collapse of the OMAs within the 5 μm illumination spot does not in itself provide an alignment stimulus since particles pull isotropically toward the glass surface. The observed outcome of cellular alignment suggests that cells sense and adapt to mechanical signals applied to subcellular regions of certain geometry. The ability to observe this unique response is attributable to the relatively small spatial scale of the OMA stimulus, which provides greater stimulation specificity compared to the whole-cell force application of cyclic strain bioreactors.

The sensitivity of cells to the time scale of mechanical stimulation remains unclear. In this work, we stimulated cells for 20 min every other day, but previous research using cyclic strain to promote myogenesis employed stimulation ranging from a few minutes every 12 h to many hours per day.[41−43] To determine if daily stimulation would produce a stronger phenotypic response in these cells, surfaces were exposed to the same stimulation parameters every day instead of every other day. Daily stimulation of cells in linear or circular geometries did not enhance alignment or markers of differentiation as compared to stimulation every other day (Figure S5). These results suggest that previously reported methods may be in excess of what is necessary to show differences between stimulated and unstimulated cells. Further study of the sensitivity of myoblasts to cyclic stretch would be a compelling topic for future study.

We hypothesize, however, that some repetitive stimulation over the 5-day study period is necessary to invoke a significant myogenic response. Figure 2 provides evidence that cells extend in response to OMA mechanical stimulation, and repeated imaging of surfaces indicates movement and rearrangement of cells as they align and differentiate. As

https://dx.doi.org/10.1021/acsami.0c08871
ACS Appl. Mater. Interfaces XXXX, XXX, XXX−XXX

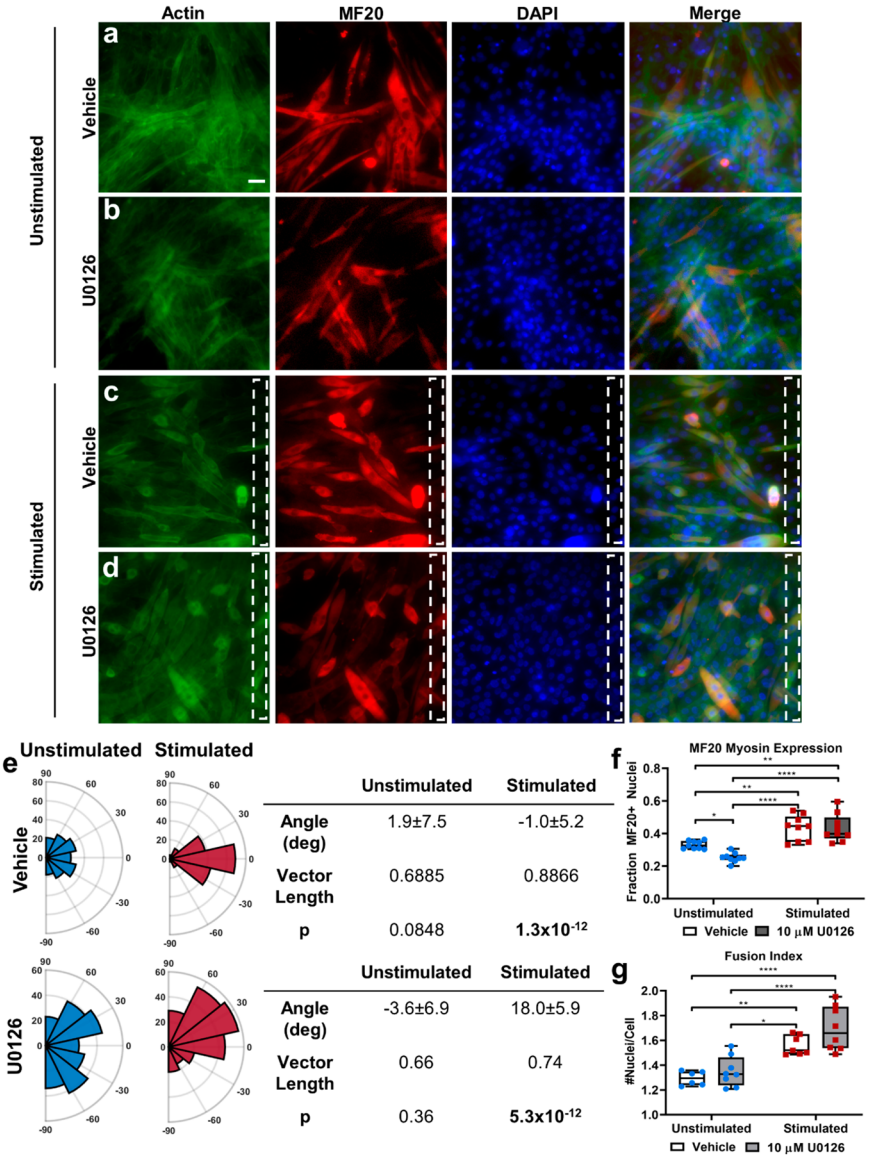

Figure 4. Role of MEK1/2 in OMA-driven myogenesis. (a–d) Representative images of myocytes stained for F-actin (phalloidin, green), sarcomeric myosin (anti-MF20, red), and nuclei (DAPI, blue). Cells were treated with a vehicle control (DMSO) (a and c) or 10 μM MEK 1/2 inhibitor U0126 (b and d) and were either unstimulated (a and b) or stimulated with NIR light at 1.1 Hz for 5 days (c and d). Scale bar = 50 μm. White dotted regions indicate stimulation area. (e) Polar histograms of myocyte and myotube alignment on untreated (top, n = 120 cells) and treated (bottom, n = 180 cells) surfaces with (right) or without (left) NIR stimulation from 3 independent experiments. Zero degree angle was set as perpendicular to the long axis of stimulation. Summary values of alignment are tabulated, showing the average alignment angle ±95% confidence interval, dispersion vector, and p value, calculated by Rayleigh's modified v-test for uniformity, with α = 0.05. (f) Box plot showing the average fraction MF20-positive nuclei under the various treatment conditions. (*) $p < 0.05$, (**) $p < 0.01$, (****) $p < 0.001$ by two-way ANOVA with Tukey's multiple comparisons, n = 9 microscopic areas from 3 independent experiments for all groups. (g) Box plot of the fusion index, quantified as the average number of nuclei per cell. (*) $p < 0.05$, (**) $p < 0.01$, (****) $p < 0.001$ by two-way ANOVA with Tukey's multiple comparisons on microscopic areas from 3 independent experiments: NIR stimulated U0126 treated n = 8; unstimulated U0126 treated n = 7; stimulated vehicle treated n = 7; unstimulated vehicle treated n = 6. Bars show range of data in both box plots.

such, each stimulation treatment would actuate a different part of a cell or a different cell altogether. This leads to several possibilities as to the role of multiple stimulation treatments: providing a second "polarization" signal to a previously actuated cell to stimulate increased alignment toward the stimulus, stimulating a previously unactuated cell to align toward the mechanical input, providing a different "polarization" signal to a previously actuated cell and cause it to realign to a different orientation, or perhaps having a "nonpolarizing" effect or no effect at all under the center of a previously stimulated or unstimulated cell.

In addition to cell migration, either random or in response to stimulation, the NIR laser is focused to induce collapse of OMAs in a 5 μm diameter spot, yet myogenesis and alignment is observed across microscopic areas of hundreds of micrometers, raising the question of how relatively few mechanically stimulated cells can direct adjacent and distal cells to differentiate. These outcomes occur in conjunction with paracrine and juxtacrine cell–cell signaling. For example, the

https://dx.doi.org/10.1021/acsami.0c08871
ACS Appl. Mater. Interfaces XXXX, XXX, XXX–XXX

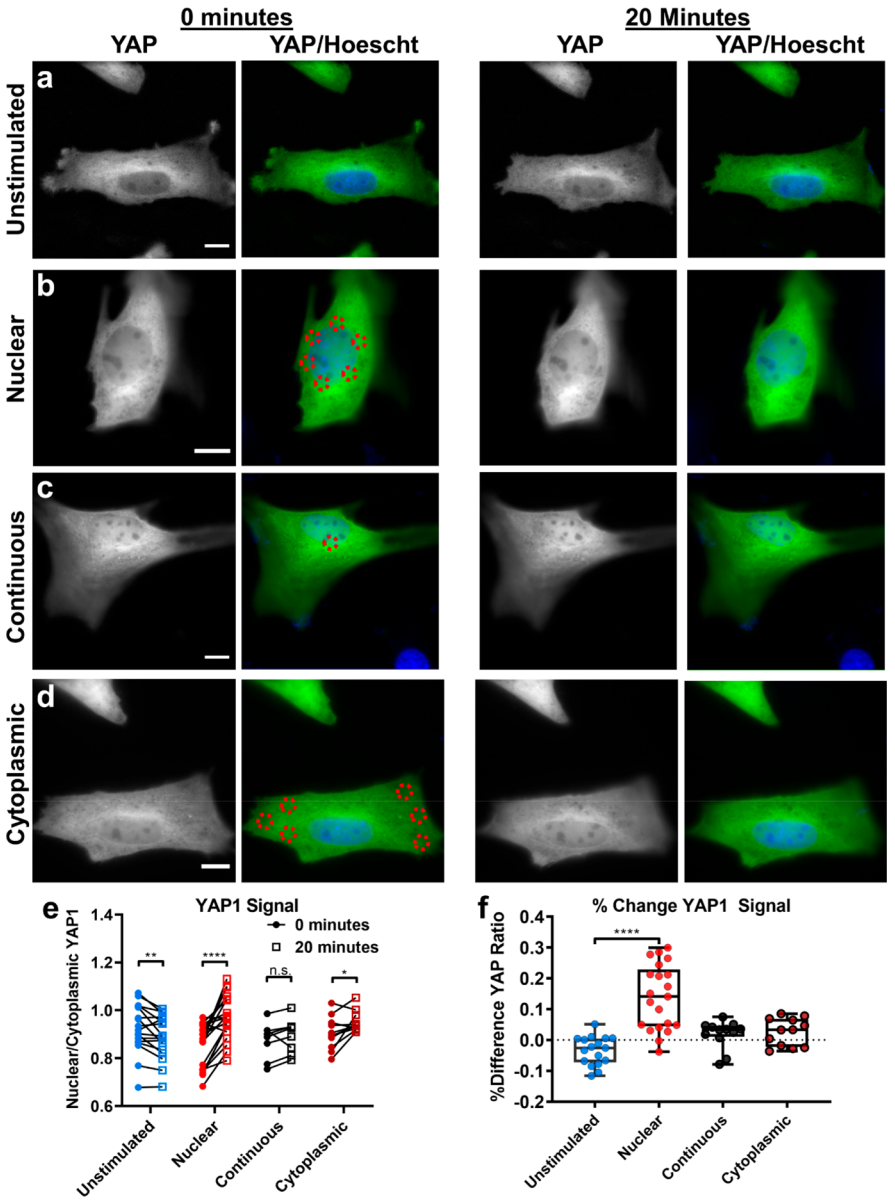

Figure 5. YAP1 nuclear localization under OMA mechanical stimulation. (a–d) Representative images of C2C12 myoblasts transfected with e-GFP-YAP1 (green), counterstained with Hoescht 33342 (blue), and exposed to either no stimulation (a), NIR stimulation near the nucleus (b), continuous NIR exposure (c), or NIR stimulation distal to the nucleus (d). Red circles indicate NIR stimulation areas. Scale bars = 10 μm. Line scans (white dashed line in images) of GFP signal in each representative image are shown at the right. (e) Plot of nuclear-to-cytoplasmic YAP signal quantified at 0 and 20 min for each stimulation condition. (*) $p < 0.05$, (**) $p < 0.01$, (****) $p < 0.0001$ by paired Student's t tests for each condition. (f) Box plot of the percent change in nuclear-to-cytoplasmic YAP signal ratios was quantified to show the relative increase or decrease in YAP signal over 20 min. (****) $p < 0.0001$ by Kruskal–Wallis nonparametric ANOVA with Dunn's multiple comparisons. Bars show range of data. Quantification for both plots was from 3 independently prepared surfaces: unstimulated $n = 18$ cells, nuclear $n = 22$ cells, continuous $n = 11$ cells, cytoplasmic $n = 12$ cells.

Notch pathway has been studied in muscle-resident stem cell activation and differentiation.[44,45] Myoblasts may use such signaling pathways or others to communicate mechanical signals with each other. Cells proximal to the NIR-exposed area may respond and align based on the mechanical stimulus and then signal adjacent cells to also align. Future work could block known myogenic cell–cell communication receptors, such as Connexin 43 or M-cadherin, or evaluate the secretome of stimulated cells to investigate the roles of these other pathways in mechanically driven myogenesis.

MEK/ERK Inhibition Dampens Mechanically-Mediated Myogenesis. In this work, we aimed to better understand the pathway by which OMAs promote myogenesis. MEK signaling is established in the literature to be active in myogenesis, and indeed, suppression of this pathway has been shown to depress myogenic factor expression and cause reduced fusion and differentiation in C2C12 cells.[46,47] We sought first to target this pathway by utilizing a MEK/ERK inhibitor, U0126. Myoblasts treated with MEK inhibitor *without* optomechanical stimulation showed no difference in alignment from unstimulated, vehicle-treated cells (Figure 4a and 4b). NIR stimulation induced a preferred alignment direction in both treated and vehicle control cells (Figure 4c and 4d). A v-test shows no preferred direction of alignment in

https://dx.doi.org/10.1021/acsami.0c08871
ACS Appl. Mater. Interfaces XXXX, XXX, XXX–XXX

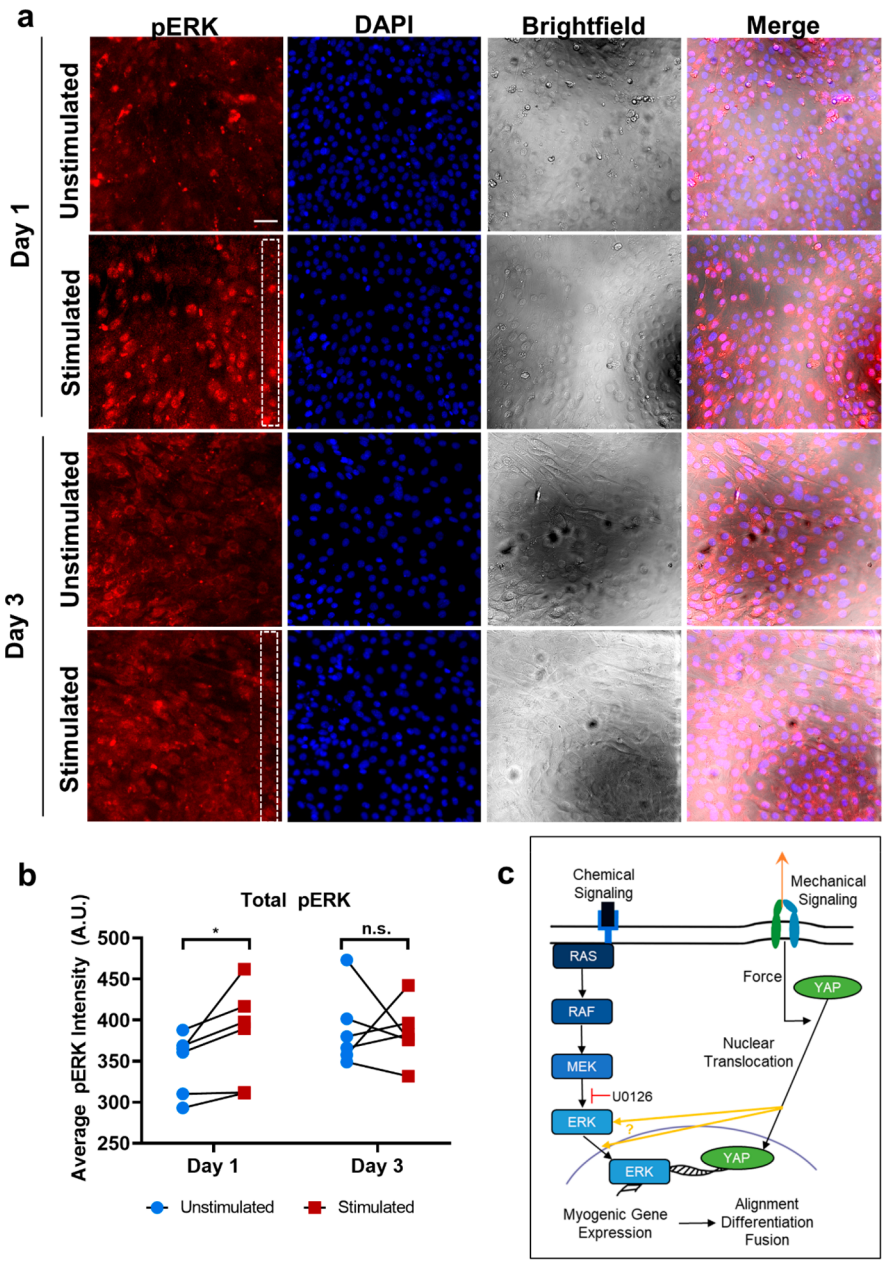

Figure 6. ERK activation as a potential mechanism for mechanically driven myogenesis. (a) Phosphorylated ERK signal in stimulated and unstimulated regions at early time points: after one stimulation (Day 1) or after two stimulation treatments (Day 3). (b) Plot showing stimulated cells have enhanced pERK expression as compared to unstimulated cells after one stimulation, and unstimulated cells gain this expression level later in myogenesis. (*) $p < 0.05$ by Wilcoxon test on $n = 2$ each stimulated and unstimulated regions on $n = 3$ independently prepared surfaces. (c) Proposed model of the interaction of ERK and YAP during OMA force application in myogenesis. Process of myogenesis is known to involve both chemical and mechanical signaling inputs. In this work, we demonstrated that applying forces to myoblast integrin receptors increases YAP translocation to the nucleus and that mechanical stimulation can overcome inhibition of MEK1/2 activity by U0126. In concert with the literature,[47,49] we propose mechanically driven myogenesis through OMAs occurs by enhancing YAP nuclear localization and driving YAP-ERK interactions to enhance myogenic gene expression, causing cellular alignment, fusion, and differentiation.

unstimulated cells with or without U0126. However, the average alignment angle of the U0126-treated and stimulated group (18°, Figure 4e) was greater than vehicle-stimulated cells in this experiment and untreated stimulated cells from other experiments, which were all aligned within 10° (Figures 3 and S4). This suggests that MEK inhibition may reduce sensitivity to the spatial arrangement of mechanical inputs.

While treatment with U0126 reduced myosin expression in unstimulated cells, expression was recovered in the presence of NIR stimulation, where no differences were observed between treated and untreated cells (two-way ANOVA with Tukey's multiple comparisons: NIR factor $p < 0.0001$, treatment factor $p = 0.060$, interaction factor p = 0.068) (Figure 4f). Finally, differentiation was verified by measuring the fusion index of treated and untreated cells. Interestingly, U0126 treatment did not suppress fusion in unstimulated cells as compared to the vehicle control, but NIR stimulation increased the average number of nuclei per cell (two-way ANOVA with Tukey's multiple comparisons: NIR factor $p < 0.0001$, U0126 factor $p = 0.050$, interaction factor $p = 0.397$) (Figure 4g). These results

https://dx.doi.org/10.1021/acsami.0c08871
ACS Appl. Mater. Interfaces XXXX, XXX, XXX−XXX

agree with other reports, where treatment with U0126 on aligned fibrous substrates also did not change myosin expression,[8] providing further support that extracellular mechanics enhances myogenesis downstream of MEK, though the biomaterials in that study provide only passive, structural cues to enhance differentiation and alignment. The alignment, myosin expression, and fusion responses together show OMA mechanical stimulation can bypass MEK activation in the myogenic signaling cascade to some degree, promoting differentiation of myoblasts as well as their alignment.

Optomechanical Stimulation Enhances YAP Nuclear Transport. To further probe the role of the MEK pathway and understand the mechanism by which cyclic strain promotes myogenesis in this system, we investigated nuclear translocation of YAP1, a mechanotransductive transcription factor[48] that has been shown to upregulate myogenic markers.[49,50] The currently proposed model of YAP nuclear entry in the literature is mediated by mechanical deformation of nuclear pores,[51] providing a hypothesis for its role in mechanically mediated myogenesis. Nuclear eGFP-YAP1 signal increased following 20 min of NIR stimulation in the region of the nucleus as compared to unstimulated cells (Figure 5a and 5b). As seen in Figure 2, continuous NIR stimulation resulted in no significant change in cellular response over time (Figure 5c). When stimulated farther from the nucleus, there was a smaller, though not statistically different, increase in nuclear YAP signal (Figure 5d). This is consistent with other work concerning YAP dynamics that demonstrated a greater increase in nuclear YAP localization when mechanical perturbation was localized to the nucleus as compared to elsewhere in the cell.[51] That study also provides a potential mechanism for the observed significant decrease in unstimulated nuclear YAP, which was expected not to change. It is likely there is some basal export rate of YAP from the nucleus, as previous work shows that while YAP accumulates in the nucleus due to direct mechanical perturbation, nuclear YAP returns to baseline levels on the order of minutes even after compression is removed and the nuclear pores are closed.[51] This strengthens our findings, indicating our transient, cyclic mechanical perturbation is sufficient to overcome YAP export rates and results in an increase in nuclear YAP over time. Overall, cells exposed to NIR light in any location or frequency trended toward an increased nuclear YAP signal, whereas unstimulated cells and continuously NIR-illuminated cells showed a decrease (i.e., more cytoplasmic YAP) or little change at all (Figure 5e and 5f). It should be noted that the results shown here are likely an underestimation of the true YAP dynamics in the cell. Addition of GFP reporter adds nearly 50% of the molecular weight of YAP to the molecule, increasing its size, and may potentially slow or limit nuclear translocation. This potential issue, along with the relatively small amount of mechanical perturbation provided by the OMAs, contributes to the relatively small changes in nuclear/cytoplasmic YAP ratios as compared to other work in the field.[51]

Cyclic strain has been previously reported to increase YAP nuclear localization in myoblasts,[52] though this is to the best of our knowledge the first report of these dynamics in myoblasts on this short time scale. It is known that extracellular strain from CSBs is transmitted to the nucleus via the actin cytoskeleton, as evidenced by changes in myogenesis when nuclear−cytoskeletal linking proteins were inhibited,[53] and our results suggest that such a mechanism allows even the small, localized strains applied by OMAs to activate mechanotransductive signals. Advancements in super-resolved confocal imaging may be able to detect the nanoscale nuclear deformations due to OMA collapse in future work.

Proposed Mechanism of Myogenic Response to OMA Stimulation. In combination with the overall recovery of the phenotype in the presence of mechanical inputs, the observed YAP response implies a role for the MEK/ERK signaling pathway in mechanically driven myogenesis. To further investigate this mechanism, surfaces were stimulated and stained after Day 1 and Day 3 for the presence of phosphorylated ERK (pERK), as Chen and colleagues demonstrated an increase in this factor in myogenic cells with high levels of YAP.[54] Only early time points in the myogenic timeline were tested here, as previous work in the field has demonstrated ERK to be most present and active in early myogenesis.[3,55] In response to OMA stimulation, myoblasts showed enhanced pERK staining compared to unstimulated regions on the same surface at Day 1, and unstimulated cells did not reach that expression level until Day 3 (Figure 6a and 6b). While MEK1/2 inhibition decreased myosin expression in cells with no OMA stimulation, the presence of mechanical inputs rescues this phenotype (Figure 4) and causes an upregulation of nuclear YAP1 (Figure 5). Such upregulation of YAP may increase activation of ERK1/2, as demonstrated by an early increase in pERK staining in mechanically stimulated cells, driving an increase in myogenic differentiation factors earlier than in unstimulated cells. In this way, mechanical stimulation may work with canonical chemical myogenic signaling pathways to enhance myogenesis (Figure 6c).

In combination with the literature, this evidence demonstrates a model for mechanically driven myogenesis. Chen and colleagues demonstrated increased phosphorylation of ERK5 as well as increased nuclear accumulation of phosphorylated ERK in cells overexpressing YAP. Furthermore, it was demonstrated that inhibition of Src, a component of the integrin signaling cascade, ablated the ability of YAP overexpression to enhance phosphorylated ERK and downstream myogenic factors.[49] These data strongly imply a role for YAP-mediated mechanical signaling in MEK/ERK myogenesis, consistent with our results. Other work has suggested that ERK1/2 may also increase the amount of YAP1 in other cell types, further supporting the connection of external force application to known chemical pathways in myogenesis.[56]

CONCLUSION

Repeated application of external forces—both in vitro and in vivo—promotes myogenesis. However, the specific cellular mechanisms of this effect are just beginning to be understood, including the sensitivity of muscle cells to mechanical stimulation. Here, we present OMAs as a method to probe single-cell effects of mechanical stimulation in a spatially and temporally dependent manner. The pro-myogenic responses observed in this study (myosin expression, alignment, fusion, YAP nuclear localization, and recovery of MEK inhibition) were seen at greater substrate strain values but at a shorter duration and smaller stimulated cell area than in the bioreactor literature, providing an unexpected result about the spatial distribution of applied strain. To the best of our knowledge, while recent work has also used responsive polymer systems to induce cellular changes via a light-driven mechanism,[57,58] the present report is the first example of such a method applied to

https://dx.doi.org/10.1021/acsami.0c08871
ACS Appl. Mater. Interfaces XXXX, XXX, XXX−XXX

myoblasts, a cell type known for its sensitivity to mechanical inputs.

It is important to note that OMA stimulation also presents some limitations. While one benefit to OMAs is the ability to stimulate and study single-cell responses to extracellular mechanics, this does preclude bulk protein and nucleic acid bioanalysis such as Western blotting or RT-PCR. Indeed, analysis methods are limited to those that can be conducted via microscopy, such as cytomorphometrics and immunofluorescence as used in this work. Future development of single-cell analysis methods such as single-cell sequencing or quantitative immunostaining/in-cell Western could work in tandem with OMAs to provide further data on the role of mechanics in myogenesis and other biological processes. As such techniques develop, OMAs can be employed as a tool to better understand how cells interact with their environment, directing the development of improved biomaterials for research and therapeutic uses.

■ ASSOCIATED CONTENT

Supporting Information

The Supporting Information is available free of charge at https://pubs.acs.org/doi/10.1021/acsami.0c08871.

Surface preparation and functionality; experimental design for 5-day myogenesis studies; evidence for integrin-mediated OMA force transmission; response of C2C12 myoblasts to different geometries of NIR mechanical stimulation; response of C2C12 myoblasts to daily NIR stimulation; supplemental video captions (PDF)

OMA actuation (AVI)

OMA actuation after 20 min (AVI)

■ AUTHOR INFORMATION

Corresponding Author

Khalid Salaita − *Wallace H. Coulter Department of Biomedical Engineering, Georgia Institute of Technology/Emory University, Atlanta, Georgia 30332, United States; Department of Chemistry, Emory University, Atlanta, Georgia 30322, United States;* orcid.org/0000-0003-4138-3477; Email: k.salaita@emory.edu

Authors

Allison N. Ramey-Ward − *Wallace H. Coulter Department of Biomedical Engineering, Georgia Institute of Technology/Emory University, Atlanta, Georgia 30332, United States*

Hanquan Su − *Department of Chemistry, Emory University, Atlanta, Georgia 30322, United States*

Complete contact information is available at: https://pubs.acs.org/10.1021/acsami.0c08871

Author Contributions

The manuscript was written through contributions of all authors. All authors have given approval to the final version of the manuscript.

Notes

The authors declare no competing financial interest.

■ ACKNOWLEDGMENTS

The authors thank Professor Young Jang at the Georgia Institute of Technology for donation of C2C12 myoblasts, Professor He Cheol Cho at Emory University for donation of Hoescht stain, and Professor Brian Dyer at Emory University for use of the DLS and spectrophotometry instruments. The authors also acknowledge Aaron T. Blanchard for advice on the use of circular statistics in this work. This work was supported by the NSF CAREER Award (1350829) and the NIH (R01-GM097399 and R01-GM124472).

■ REFERENCES

(1) Chal, J.; Pourquié, O. Making Muscle: Skeletal Myogenesis in Vivo and in Vitro. *Development (Cambridge, U. K.)* **2017**, *144*, 2104−2122.

(2) Sabourin, L. A.; Rudnicki, M. A. The Molecular Regulation of Myogenesis. *Clin. Genet.* **2000**, *57*, 16−25.

(3) Coolican, S. A.; Samuel, D. S.; Ewton, D. Z.; McWade, F. J.; Florini, J. R. The Mitogenic and Myogenic Actions of Insulin-like Growth Factors Utilize Distinct Signaling Pathways. *J. Biol. Chem.* **1997**, *272* (10), 6653−6662.

(4) Jo, C.; Cho, S. J.; Jo, S. A. Mitogen-Activated Protein Kinase Kinase 1 (MEK1) Stabilizes MyoD through Direct Phosphorylation at Tyrosine 156 during Myogenic Differentiation. *J. Biol. Chem.* **2011**, *286* (21), 18903−18913.

(5) Wolf, M. T.; Daly, K. A.; Reing, J. E.; Badylak, S. F. Biologic Scaffold Composed of Skeletal Muscle Extracellular Matrix. *Biomaterials* **2012**, *33* (10), 2916−2925.

(6) Engler, A. J.; Griffin, M. A.; Sen, S.; Bönnemann, C. G.; Sweeney, H. L.; Discher, D. E. Myotubes Differentiate Optimally on Substrates with Tissue-like Stiffness: Pathological Implications for Soft or Stiff Microenvironments. *J. Cell Biol.* **2004**, *166* (6), 877−887.

(7) Mayer, U.; Saher, G.; Fässler, R.; Bornemann, A.; Echtermeyer, F.; von der Mark, H.; Miosge, N.; Pösch, E.; von der Mark, K. Absence of Integrin Alpha 7 Causes a Novel Form of Muscular Dystrophy. *Nat. Genet.* **1997**, *17* (3), 318−323.

(8) McClure, M. J.; Clark, N. M.; Hyzy, S. L.; Chalfant, C. E.; Olivares-Navarrete, R.; Boyan, B. D.; Schwartz, Z. Role of Integrin A7β1 Signaling in Myoblast Differentiation on Aligned Polydioxanone Scaffolds. *Acta Biomater.* **2016**, *39*, 44−54.

(9) Prüller, J.; Mannhardt, I.; Eschenhagen, T.; Zammit, P. S.; Figeac, N. Satellite Cells Delivered in Their Niche Efficiently Generate Functional Myotubes in Three-Dimensional Cell Culture. *PLoS One* **2018**, *13* (9), No. e0202574.

(10) Matsumoto, T.; Sasaki, J. I.; Alsberg, E.; Egusa, H.; Yatani, H.; Sohmura, T. Three-Dimensional Cell and Tissue Patterning in a Strained Fibrin Gel System. *PLoS One* **2007**, *2* (11), No. e1211.

(11) Sharif, S.; Thomas, J. M.; Donley, D. A.; Gilleland, D. L.; Bonner, D. E.; McCrory, J. L.; Hornsby, W. G.; Zhao, H.; Lively, M. W.; Hornsby, J. A. A.; Alway, S. E. Resistance Exercise Reduces Skeletal Muscle Cachexia and Improves Muscle Function in Rheumatoid Arthritis. *Case Rep. Med.* **2011**, *2011*, 1.

(12) Jansen, M.; Van Alfen, N.; Geurts, A. C. H.; De Groot, I. J. M. Assisted Bicycle Training Delays Functional Deterioration in Boys with Duchenne Muscular Dystrophy: The Randomized Controlled Trial "No Use Is Disuse". *Neurorehabil. Neural Repair* **2013**, *27* (9), 816−827.

(13) Nordemar, R.; Edström, L.; Ekblom, B. Changes in Muscle Fibre Size and Physical Performance in Patients with Rheumatoid Arthritis after Short-Term Physical Training. *Scand. J. Rheumatol.* **1976**, *5* (2), 70−76.

(14) Egusa, H.; Kobayashi, M.; Matsumoto, T.; Sasaki, J.-I.; Uraguchi, S.; Yatani, H. Application of Cyclic Strain for Accelerated Skeletal Myogenic Differentiation of Mouse Bone Marrow-Derived Mesenchymal Stromal Cells with Cell Alignment. *Tissue Eng., Part A* **2013**, *19* (5−6), 770−782.

(15) Pennisi, C. P.; Olesen, C. G.; de Zee, M.; Rasmussen, J.; Zachar, V. Uniaxial Cyclic Strain Drives Assembly and Differentiation of Skeletal Myocytes. *Tissue Eng., Part A* **2011**, *17* (19−20), 2543−2550.

(16) Chang, Y. J.; Chen, Y. J.; Huang, C. W.; Fan, S. C.; Huang, B. M.; Chang, W. T.; Tsai, Y. S.; Su, F. C.; Wu, C. C. Cyclic Stretch

Facilitates Myogenesis in C2C12 Myoblasts and Rescues Thiazolidinedione-Inhibited Myotube Formation. *Front. Bioeng. Biotechnol.* **2016**, *4* (27), 1−8.
(17) Hu, Y.; You, J.-O.; Aizenberg, J. Micropatterned Hydrogel Surface with High-Aspect-Ratio Features for Cell Guidance and Tissue Growth. *ACS Appl. Mater. Interfaces* **2016**, *8*, 21939−21945.
(18) Formigli, L.; Meacci, E.; Sassoli, C.; Chellini, F.; Giannini, R.; Quercioli, F.; Tiribilli, B.; Squecco, R.; Bruni, P.; Francini, F.; Zecchi-Orlandini, S. Sphingosine 1-Phosphate Induces Cytoskeletal Reorganization in C2C12 Myoblasts: Physiological Relevance for Stress Fibres in the Modulation of Ion Current through Stretch-Activated Channels. *J. Cell Sci.* **2005**, *118* (6), 1161−1171.
(19) Montel, L.; Sotiropoulos, A.; Henon, S. The Nature and Intensity of Mechanical Stimulation Drive Different Dynamics of MRTF-A Nuclear Redistribution after Actin Remodeling in Myoblasts. *PLoS One* **2019**, *14* (3), No. e0214385.
(20) Zhao, J.; Su, H.; Vansuch, G. E.; Liu, Z.; Salaita, K.; Dyer, R. B. Localized Nanoscale Heating Leads to Ultrafast Hydrogel Volume-Phase Transition. *ACS Nano* **2019**, *13* (1), 515−525.
(21) Liu, Z.; Liu, Y.; Chang, Y.; Seyf, H. R.; Henry, A.; Mattheyses, A. L.; Yehl, K.; Zhang, Y.; Huang, Z.; Salaita, K. Nanoscale Optomechanical Actuators for Controlling Mechanotransduction in Living Cells. *Nat. Methods* **2016**, *13* (2), 143−146.
(22) Mercer, S. E.; Ewton, D. Z.; Deng, X.; Lim, S.; Mazur, T. R.; Friedman, E. Mirk/Dyrk1B Mediates Survival during the Differentiation of C2C12 Myoblasts. *J. Biol. Chem.* **2005**, *280* (27), 25788−25801.
(23) Basu, S.; Totty, N. F.; Irwin, M. S.; Sudol, M.; Downward, J. Akt Phosphorylates the Yes-Associated Protein, YAP, to Induce Interaction with 14−3-3 and Attenuation of P73-Mediated Apoptosis. *Mol. Cell* **2003**, *11* (1), 11−23.
(24) Bader, D.; Masaki, T.; Fischman, D. A. Immunochemical Analysis of Myosin Heavy Chain during Avian Myogenesis in Vivo and in Vitro. *J. Cell Biol.* **1982**, *95* (3), 763−770.
(25) Berens, P. CircStat: A Matlab Toolbox for Circular Statistics. *J. Stat. Software* **2009**, *31* (10). DOI: 10.18637/jss.v031.i10
(26) Su, H.; Liu, Z.; Liu, Y.; Ma, V. P.-Y.; Blanchard, A.; Zhao, J.; Galior, K.; Dyer, R. B.; Salaita, K. Light-Responsive Polymer Particles as Force Clamps for the Mechanical Unfolding of Target Molecules. *Nano Lett.* **2018**, *18* (4), 2630−2636.
(27) Kubota, K.; Hamano, K.; Kuwahara, N.; Fujishige, S.; Ando, I. Characterization of Poly(N-Isopropylmethacrylamide) in Water. *Polym. J.* **1990**, *22*, 1051−1057.
(28) Duracher, D.; Elaissari, A.; Pichot, C. Characterization of Cross-Linked Poly(N-Isopropylmethacrylamide) Microgel Latexes. *Colloid Polym. Sci.* **1999**, *277*, 905−913.
(29) Yilgor Huri, P.; Cook, C.A.; Hutton, D.L.; Goh, B.C.; Gimble, J.M.; DiGirolamo, D.J.; Grayson, W.L. Biophysical Cues Enhance Myogenesis of Human Adipose Derived Stem/Stromal Cells. *Biochem. Biophys. Res. Commun.* **2013**, *438*, 180−185.
(30) Andersen, J. I.; Juhl, M.; Nielsen, T.; Emmersen, J.; Fink, T.; Zachar, V.; Pennisi, C. P. Uniaxial Cyclic Strain Enhances Adipose-Derived Stem Cell Fusion with Skeletal Myocytes. *Biochem. Biophys. Res. Commun.* **2014**, *450* (2), 1083−1088.
(31) Chandran, R.; Knobloch, T. J.; Anghelina, M.; Agarwal, S. Biomechanical Signals Upregulate Myogenic Gene Induction in the Presence or Absence of Inflammation. *Am. J. Physiol. Physiol.* **2007**, *293* (1), C267−C276.
(32) Liu, J.; Liu, J.; Mao, J.; Yuan, X.; Lin, Z.; Li, Y. Caspase-3-Mediated Cyclic Stretch-Induced Myoblast Apoptosis via a Fas/FasL-Independent Signaling Pathway during Myogenesis. *J. Cell. Biochem.* **2009**, *107* (4), 834−844.
(33) Burattini, S.; Ferri, R.; Battistelli, M.; Curci, R.; Luchetti, F.; Falcieri, E. C2C12 Murine Myoblasts as a Model of Skeletal Muscle Development: Morpho-Functional Characterization. *Eur. J. Histochem.* **2004**, *48* (3), 223−233.
(34) Johnston, A. P. W.; Baker, J.; De Lisio, M.; Parise, G. Skeletal Muscle Myoblasts Possess a Stretch-Responsive Local Angiotensin Signalling System. *JRAAS* **2011**, *12* (2), 75−84.
(35) Naskar, S.; Kumaran, V.; Basu, B. On the Origin of Shear Stress Induced Myogenesis Using PMMA Based Lab-on-Chip. *ACS Biomater. Sci. Eng.* **2017**, *3* (6), 1154−1171.
(36) Heher, P.; Maleiner, B.; Prüller, J.; Teuschl, A. H.; Kollmitzer, J.; Monforte, X.; Wolbank, S.; Redl, H.; Rünzler, D.; Fuchs, C. A Novel Bioreactor for the Generation of Highly Aligned 3D Skeletal Muscle-like Constructs through Orientation of Fibrin via Application of Static Strain. *Acta Biomater.* **2015**, *24*, 251−265.
(37) Comisar, W. A.; Mooney, D. J.; Linderman, J. J. Integrin Organization: Linking Adhesion Ligand Nanopatterns with Altered Cell Responses. *J. Theor. Biol.* **2011**, *274* (1), 120−130.
(38) Cavalcanti-Adam, E. A.; Volberg, T.; Micoulet, A.; Kessler, H.; Geiger, B.; Spatz, J. P. Cell Spreading and Focal Adhesion Dynamics Are Regulated by Spacing of Integrin Ligands. *Biophys. J.* **2007**, *92* (8), 2964−2974.
(39) Jiao, A.; Moerk, C. T.; Penland, N.; Perla, M.; Kim, J.; Smith, A. S. T.; Murry, C. E.; Kim, D.-H. Regulation of Skeletal Myotube Formation and Alignment by Nanotopographically Controlled Cell-Secreted Extracellular Matrix. *J. Biomed. Mater. Res., Part A* **2018**, *106* (6), 1543−1551.
(40) Patel, K. H.; Dunn, A. J.; Talovic, M.; Haas, G. J.; Marcinczyk, M.; Elmashhady, H.; Kalaf, E. G.; Sell, S. A.; Garg, K. Aligned Nanofibers of Decellularized Muscle ECM Support Myogenic Activity in Primary Satellite Cells in Vitro. *Biomed. Mater.* **2019**, *14* (3), No. 035010.
(41) Cezar, C. A.; Roche, E. T.; Vandenburgh, H. H.; Duda, G. N.; Walsh, C. J.; Mooney, D. J. Biologic-Free Mechanically Induced Muscle Regeneration. *Proc. Natl. Acad. Sci. U. S. A.* **2016**, *113* (6), 1534−1539.
(42) Huri, P. Y.; Morrissette-McAlmon, J.; Grayson, W. L. *Myogenic Differentiation of ASCs Using Biochemical and Biophysical Induction*; Humana Press: New York, 2018; pp 123−135.
(43) Salazar, B. H.; Cashion, A. T.; Dennis, R. G.; Birla, R. K. Development of a Cyclic Strain Bioreactor for Mechanical Enhancement and Assessment of Bioengineered Myocardial Constructs. *Cardiovasc. Eng. Technol.* **2015**, *6* (4), 533−545.
(44) Sun, D.; Li, H.; Zolkiewska, A. The Role of Delta-like 1 Shedding in Muscle Cell Self-Renewal and Differentiation. *J. Cell Sci.* **2008**, *121* (22), 3815−3823.
(45) Conboy, I. M.; Rando, T. A. The Regulation of Notch Signaling Controls Satellite Cell Activation and Cell Fate Determination in Postnatal Myogenesis. *Dev. Cell* **2002**, *3* (3), 397−409.
(46) Li, J.; Johnson, S. E. ERK2 Is Required for Efficient Terminal Differentiation of Skeletal Myoblasts. *Biochem. Biophys. Res. Commun.* **2006**, *345* (4), 1425−1433.
(47) Gredinger, E.; Gerber, A. N.; Tamir, Y.; Tapscott, S. J.; Bengal, E. Mitogen-Activated Protein Kinase Pathway Is Involved in the Differentiation of Muscle Cells. *J. Biol. Chem.* **1998**, *273* (17), 10436−10444.
(48) Dupont, S.; Morsut, L.; Aragona, M.; Enzo, E.; Giulitti, S.; Cordenonsi, M.; Zanconato, F.; Le Digabel, J.; Forcato, M.; Bicciato, S.; Elvassore, N.; Piccolo, S. Role of YAP/TAZ in Mechanotransduction. *Nature* **2011**, *474* (7350), 179−184.
(49) Chen, T.-H.; Chen, C.-Y.; Wen, H.-C.; Chang, C.-C.; Wang, H.-D.; Chuu, C.-P.; Chang, C.-H. YAP Promotes Myogenic Differentiation *via* the MEK5-ERK5 Pathway. *FASEB J.* **2017**, *31* (7), 2963−2972.
(50) Watt, K. I.; Judson, R. N.; Medlow, P.; Reid, K.; Kurth, T. B.; Burniston, J. G.; Ratkevicius, A.; De Bari, C.; Wackerhage, H. Yap Is a Novel Regulator of C2C12 Myogenesis. *Biochem. Biophys. Res. Commun.* **2010**, *393* (4), 619−624.
(51) Elosegui-Artola, A.; Andreu, I.; Beedle, A. E. M.; Lezamiz, A.; Uroz, M.; Kosmalska, A. J.; Oria, R.; Kechagia, J. Z.; Rico-Lastres, P.; Le Roux, A.-L.; Shanahan, C. M.; Trepat, X.; Navajas, D.; Garcia-Manyes, S.; Roca-Cusachs, P. Force Triggers YAP Nuclear Entry by Regulating Transport across Nuclear Pores. *Cell* **2017**, *171* (6), 1397−1410.
(52) Bertrand, A. T.; Ziaei, S.; Ehret, C.; Lè Ne Duchemin, H.; Mamchaoui, K.; Bigot, A.; Le Mayer, M.; Quijano-Roy, S.; Desguerre,

I.; Lainé, J.; Ben Yaou, R.; Le Bonne, G.; Coirault, C. Cellular Microenvironments Reveal Defective Mechanosensing Responses and Elevated YAP Signaling in LMNA-Mutated Muscle Precursors. *J. Cell Sci.* **2014**, *127* (13), 2873−2884.
(53) Brosig, M.; Ferralli, J.; Gelman, L.; Chiquet, M.; Chiquet-Ehrismann, R. Interfering with the Connection between the Nucleus and the Cytoskeleton Affects Nuclear Rotation, Mechanotransduction and Myogenesis. *Int. J. Biochem. Cell Biol.* **2010**, *42* (10), 1717−1728.
(54) Chen, T.-H.; Chen, C.-Y.; Wen, H.-C.; Chang, C.-C.; Wang, H.-D.; Chuu, C.-P.; Chang, C.-H. YAP Promotes Myogenic Differentiation *via* the MEK5-ERK5 Pathway. *FASEB J.* **2017**, *31* (7), 2963−2972.
(55) McClure, M. J.; Ramey, A. N.; Rashid, M.; Boyan, B. D.; Schwartz, Z. Integrin A7 Signaling Regulates Connexin 43, M-Cadherin and Myoblast Fusion. *Am. J. Physiol. Physiol.* **2019**, *316* (6), C876−C887.
(56) You, B.; Yang, Y. L.; Xu, Z.; Dai, Y.; Liu, S.; Mao, J. H.; Tetsu, O.; Li, H.; Jablons, D. M.; You, L. Inhibition of ERK1/2 down-Regulates the Hippo/YAP Signaling Pathway in Human NSCLC Cells. *Oncotarget* **2015**, *6* (6), 4357−4368.
(57) Chandorkar, Y.; Castro Nava, A.; Schweizerhof, S.; Van Dongen, M.; Haraszti, T.; Köhler, J.; Zhang, H.; Windoffer, R.; Mourran, A.; Möller, M.; De Laporte, L. Cellular Responses to Beating Hydrogels to Investigate Mechanotransduction. *Nat. Commun.* **2019**, *10* (1), 4027.
(58) Sutton, A.; Shirman, T.; Timonen, J. V. I.; England, G. T.; Kim, P.; Kolle, M.; Ferrante, T.; Zarzar, L. D.; Strong, E.; Aizenberg, J. Photothermally Triggered Actuation of Hybrid Materials as a New Platform for in Vitro Cell Manipulation. *Nat. Commun.* **2017**, *8*, 14700.

https://dx.doi.org/10.1021/acsami.0c08871
ACS Appl. Mater. Interfaces XXXX, XXX, XXX−XXX